

Continuous-Flow Methyl Methacrylate Synthesis over Gallium-Based Bifunctional Catalysts

Jacopo De Maron, Martina Eberle, Fabrizio Cavani, Francesco Basile, Nikolaos Dimitratos, Pedro J. Maireles-Torres, Enrique Rodriguez-Castellón, and Tommaso Tabanelli*

Cite This: *ACS Sustainable Chem. Eng.* 2021, 9, 1790–1803

Read Online

ACCESS |



Metrics & More



Article Recommendations

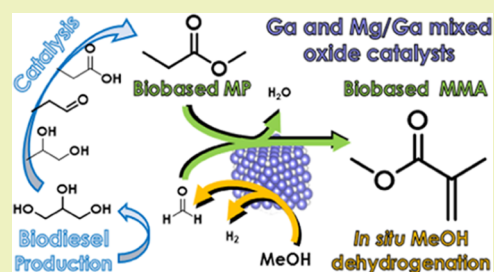


Supporting Information

ABSTRACT: This paper reports on a systematic study on the catalytic gas-phase synthesis of methyl methacrylate (MMA) by means of the hydroxymethylation and dehydration of methyl propionate (MP) with formaldehyde (FAL), the latter being produced *in situ* by methanol (MeOH) dehydrogenation. This represents a promising variant of the current industrial Alpha process in which pure FAL is fed, alongside MP, into a gas-phase fixed-bed reactor filled with a supported Cs_2O catalyst. In this way, an alternative process avoiding the need to feed carcinogenic FAL has been developed by feeding MeOH vapors onto a catalyst with dehydrogenating properties. For this purpose, an innovative Ga oxide-based bifunctional catalytic system is herein described for the first time for this peculiar application. Its catalytic performance and its chemical–physical features were investigated and evaluated to explain structure–activity relationships. Side reactions, MP ketonization, and MMA hydrogenation via H-transfer were accelerated in the presence of strong basic sites. The commercial, low-surface-area $\beta\text{-Ga}_2\text{O}_3$ catalyst showed a strong dehydrogenating activity and the highest selectivity toward MMA due to its weak basicity. However, deactivation was observed due to (i) the deposition of carbonaceous species onto surface acidic sites, as evidenced by means of X-ray photoelectron spectroscopy (XPS) analysis, and (ii) the loss of specific surface area. On the other hand, Ga^{3+} could be easily incorporated into MgO by means of a simple co-precipitation technique, leading to Mg/Ga mixed oxides with a high specific surface area. When relatively small amounts of Ga^{3+} were used (e.g., in a Mg/Ga mixed oxide with the Mg/Ga atomic ratio = 10), the catalyst was much more active in MeOH dehydrogenation with respect to pure MgO. Moreover, the presence of Ga^{3+} ions reduced the density and strength of the basic sites while increasing the selectivity toward MMA by decreasing the occurrence of the H-transfer and ketonization reactions, which, conversely, readily occurred on highly basic MgO. On the other hand, the Mg/Ga mixed oxide with Mg/Ga = 10 showed a weaker acidity compared to $\beta\text{-Ga}_2\text{O}_3$ and better stability due to limited coking. These results have shown both the potential and limitations of this alternative strategy. In particular, a more selective transformation of methanol to MMA needs to be achieved to allow the applicability of the proposed strategy on a bigger scale. Therefore, future efforts will be devoted to catalyst and condition optimization, also with the aim of limiting methanol unselective decomposition reactions.

Its catalytic performance and its chemical–physical features were investigated and evaluated to explain structure–activity relationships. Side reactions, MP ketonization, and MMA hydrogenation via H-transfer were accelerated in the presence of strong basic sites. The commercial, low-surface-area $\beta\text{-Ga}_2\text{O}_3$ catalyst showed a strong dehydrogenating activity and the highest selectivity toward MMA due to its weak basicity. However, deactivation was observed due to (i) the deposition of carbonaceous species onto surface acidic sites, as evidenced by means of X-ray photoelectron spectroscopy (XPS) analysis, and (ii) the loss of specific surface area. On the other hand, Ga^{3+} could be easily incorporated into MgO by means of a simple co-precipitation technique, leading to Mg/Ga mixed oxides with a high specific surface area. When relatively small amounts of Ga^{3+} were used (e.g., in a Mg/Ga mixed oxide with the Mg/Ga atomic ratio = 10), the catalyst was much more active in MeOH dehydrogenation with respect to pure MgO. Moreover, the presence of Ga^{3+} ions reduced the density and strength of the basic sites while increasing the selectivity toward MMA by decreasing the occurrence of the H-transfer and ketonization reactions, which, conversely, readily occurred on highly basic MgO. On the other hand, the Mg/Ga mixed oxide with Mg/Ga = 10 showed a weaker acidity compared to $\beta\text{-Ga}_2\text{O}_3$ and better stability due to limited coking. These results have shown both the potential and limitations of this alternative strategy. In particular, a more selective transformation of methanol to MMA needs to be achieved to allow the applicability of the proposed strategy on a bigger scale. Therefore, future efforts will be devoted to catalyst and condition optimization, also with the aim of limiting methanol unselective decomposition reactions.

KEYWORDS: methyl methacrylate, methyl propionate, methanol, hydroxy-methylation, alkylation, gas phase, gallium oxide, magnesium/gallium mixed oxides



INTRODUCTION

Methyl methacrylate (MMA), the monomer for poly(methyl methacrylate) production (1.6 Mt/year in 2010),¹ with an expected global production of 4.8 Mt/year in 2020,² is a chemical compound halfway between commodities and specialties.

In spite of the several production processes developed,² most MMA is still produced by the oldest and less sustainable acetone cyanohydrin (ACH) process developed by DuPont and ICI in the 1930s.² This process uses hazardous reagents and intermediates (e.g., HCN, H_2SO_4 , ACH), produces large amounts of inorganic waste (NH_4HSO_4), is energy-intensive, and depends entirely on fossil feedstock.

The process innovation driven by the increased demand for sustainability led to the development of the Lucite α process,^{3,4}

where methyl propionate (MP) is reacted with formaldehyde (FAL) in a fixed-bed gas-phase reactor at 300–400 °C on a catalyst made of Cs_2O supported on SiO_2 . Both MP and FAL are prepared in the same production site with the aim of increasing process integration: MP is produced by the methoxycarbonylation of ethylene with CO and methanol (MeOH), while anhydrous FAL is prepared by the oxidative dehydrogenation of MeOH followed by distillation.

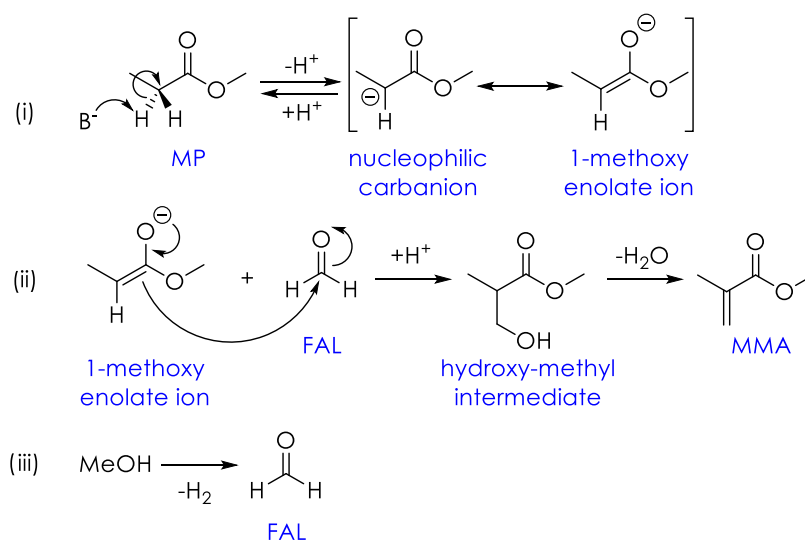
Received: October 29, 2020

Revised: January 2, 2021

Published: January 20, 2021



Scheme 1. (i) MP Activation by Base-Catalyzed α -Hydrogen Abstraction; (ii) MP Hydroxymethylation with FAL and Dehydration to MMA; and (iii) Production of FAL In Situ by Means of MeOH Dehydrogenation



This process is extremely selective and uses cheap feedstock (ethylene, CO, and MeOH), and, as water is the only co-product, its atom economy is nearly 100%. However, it depends on fossil feedstock and requires anhydrous FAL because higher amounts of water were found to be detrimental to catalyst activity and long-term stability.³ The latter requirement contributes to increasing operation costs; moreover, the storage and use of large volumes of FAL present several safety concerns because FAL has been recently classified as a group 1 carcinogen (carcinogenic for humans) by the International Agency for Research on Cancer (IARC).⁵

To improve the sustainability of MMA production, it would be advisable to develop a process based on renewable feedstocks that avoids the direct use of FAL, and indeed, some processes have already been patented. As an example, a process involving a synthetic pathway similar to the one of the Alpha process but using CO and H₂ obtained from the gasification of renewables⁶ and ethylene produced by the dehydration of bioethanol⁷ for the preparation of MP and MeOH has been recently described.⁸ The same patent also describes a variant of the same process where dimethoxymethane is used in place of FAL as a safer reactant. Other strategies toward biobased MMA involve its synthesis from itaconic acid⁹ and the synthesis of MP from a renewable building block such as the glycerol co-produced during biodiesel production,¹⁰ either through a multistep catalytic process^{11,12} or by means of fermentation¹³ and esterification.

On the other hand, renewable MeOH can be obtained either from the biosyngas produced by the gasification of lignocellulosic biomass⁶ or by reacting CO₂ and H₂ produced by means of the aqueous phase reforming of renewable raw materials.^{14,15} For these reasons, the Alpha process could be carried out with a renewable feed with minor adjustments, something that is highly desirable.

The most widely accepted mechanism for MP hydroxymethylation with FAL involves the following steps: (i) the abstraction of an acidic α -hydrogen from the ester promoted by the catalyst's basic sites (e.g., O²⁻ ions of Cs₂O in the Alpha process) and the formation of a nucleophilic carbanion or enolate ion and (ii) a nucleophilic attack on FAL from this

activated form of MP, which leads to a hydroxymethyl intermediate that finally dehydrates to MMA (Scheme 1).^{16–18}

Considering that the need for an inlet stream of pure FAL is the main drawback of the Alpha process, the *in situ* production of this reactant in a closed and strictly controlled environment (e.g., the same reactor where the hydroxymethylation of MP with FAL takes place) is a promising alternative strategy. This “one-pot” synthetic procedure would avoid the presence of FAL in the upstream stages of the process, while the *in situ* formed FAL would be completely converted at the reaction temperature by either reacting with MP or decomposing into less dangerous gaseous products and finally limiting the FAL concentration in the outlet stream as well.

FAL is industrially produced¹⁹ by either the oxidative dehydrogenation of MeOH over a silver catalysts or its oxidation over an Fe/Mo/O catalyst. The *in situ* oxidation of mixtures of bioalcohols has also been described in both the patent and academic literature (e.g., MeOH/EtOH and MeOH/PrOH mixtures were oxidized *in situ* to FAL/acetaldehyde and FAL/propionaldehyde (PAL) for the synthesis of acrolein²⁰ and methacrolein,²¹ respectively, by means of aldol condensation). However, MeOH oxidation co-produces H₂O, which not only favors the reverse reaction of MP coupling with FAL but can also lead to the hydrolysis of MP into propionic acid (PA) and carboxylic acids, which are known to be much more reactive toward the parasitic reaction of ketonization with respect to esters.²² The use of dimethoxymethane as a source of anhydrous FAL has been described by several authors,^{8,23} but others claimed that this reactant is undesirable because it may lead to the formation of H₂O under reaction conditions.²⁴ Furthermore, oxidation processes often suffer from a reduced selectivity due to unselective oxidations occurring on both the reactants and the product (e.g., decomposition/total oxidation of the very reactive FAL produced *in situ* and unselective oxidation of MP and MMA). Such unwanted reactions would eventually add to those that already occur in the absence of oxygen and water. Therefore, in this work, it has been preferred to investigate the production of FAL *in situ* by means of MeOH dehydrogenation, thus avoiding the production of water as a co-product.

FAL can be obtained *in situ* from MeOH on catalysts possessing either redox or basic features, the former usually being active at significantly lower temperatures. The choice of redox components should be narrowed to the more selective ones for the nonoxidative MeOH dehydrogenation (particularly oxides, sulfides, and phosphates of Ag, Cu, and Zn).^{25,26} Basic oxides such as MgO catalyze the nonoxidative dehydrogenation of MeOH only, even though temperatures as high as 400–450 °C are required.^{27–29}

The scientific literature regarding the target reaction (MMA synthesis from MP and FAL produced *in situ* from MeOH dehydrogenation) is scarce, and, to the best of our knowledge, only two papers covering this topic have been published, both focusing on bifunctional basic/redox catalysts.

Ai investigated a catalyst consisting of Ag⁺, Cs⁺, and Zr⁴⁺ supported on SiO₂.³⁰ Cs and Ag oxides provide the basicity required for MP activation and the redox activity for MeOH dehydrogenation, respectively, while Zr⁴⁺ acts as a promoter. The authors pointed out (i) that the catalyst activity decreased with an increase of the time on stream due to the reduction of Ag oxide to metallic Ag and (ii) that the addition of oxygen to the feed is required to maintain a stable catalyst activity. Moreover, at the beginning of the reaction, the sole product was methyl isobutyrate (MIB), which disappeared after a few hours, giving way to MMA.

On the other hand, Ueda investigated a MgO-based catalyst impregnated with Mn²⁺ ions.³¹ It was found that a Mn²⁺ loading up to 5 wt % boosted both MP conversion (from 5 to 10%) and MMA selectivity (from 8 to 60%) compared to pure MgO. In this case, three byproducts were reported: MIB (in agreement with Ai³⁰), 3-pentanone (3Pa), and 2-methyl-3-pentanone (M-3Pe), the latter produced by the hydroxymethylation/dehydration of 3Pa with FAL (in agreement with Bailey et al.).³² To sum up, the available literature does not present detailed information about the reaction scheme, side reactions, and structure–activity relationships governing catalyst activity, selectivity, and stability, thus struggling to grasp the big picture of such an industrially significant process.

In this paper, we report the catalytic performance of three novel catalytic systems based on Ga³⁺ (Ga₂O₃ and two Mg/Ga mixed oxides characterized by different Mg/Ga atomic ratios: 10 and 20, respectively) for the one-pot synthesis of MMA from MeOH and MP, with a particular focus on the complex reaction scheme arising from the simultaneous occurrence of the two target reactions (MeOH dehydrogenation to FAL and the consecutive hydroxymethylation of MP to produce MMA) and main side reactions (ketonization and catalytic transfer hydrogenation (CTH) reductions). Moreover, the structure–activity relationship that links redox and acid/base properties to the catalytic activity, selectivity, and deactivation behavior of the catalysts was also systematically and thoroughly investigated.

MATERIALS AND METHODS

Catalyst Preparation. Henceforth in the text, catalysts will be referred to as follows: MgO and Ga₂O₃ for pure metal oxides; “Mg/Ga-10” and “Mg/Ga-20” for the mixed metal oxides with Mg/Ga atomic ratios of 10 and 20, respectively; and “Mg/Ga-mix” for the physical mixture of MgO and Ga₂O₃ with the Mg/Ga atomic ratio equal to 10 (9.1 mol % Ga, 90.9 mol % MgO).

Ga₂O₃ is a commercial reference material (Alfa Aesar, 99.99%).

MgO was synthesized according to a well-known precipitation procedure reported in the [Supporting Information](#).

The MgO/Ga₂O₃ physical mixture with the Mg/Ga atomic ratio = 10 was prepared by thoroughly grinding the powders of both the synthetic MgO and commercial Ga₂O₃ together in an agate mortar for 10 min.

Mg/Ga-10 and Mg/Ga-20 were synthesized according to a coprecipitation technique adapted from that used for the synthesis of MgO. The main differences lie in the preparation of the metal precursor solutions and in the pH of the synthesis, which was adjusted to 8.5 to avoid the solubilization of gallium hydroxides and Mg/Ga hydrotalcites, which become soluble at a pH above 9. Further details are reported in the [Supporting Information](#).

The catalyst pellets were obtained by pressing the powders into a self-sustaining disk (≈30 mm in diameter and 1 mm in height), which was then crushed through a 30-mesh sieve placed on top of a 60-mesh sieve. After crushing, the fraction of pellets with granulometry between 30 and 60 meshes trapped between the two sieves was collected and loaded inside the reactor.

Catalyst Characterization. X-ray diffraction (XRD) powder patterns of the catalysts were recorded with Cu K α radiation ($\lambda = 1.54178$ Å, Ni-filtered) on a Philips X'Pert diffractometer in Bragg–Brentano geometry, equipped with a pulse height analyzer and a secondary curved graphite-crystal monochromator. The crystallinity of the different materials was compared by calculating the average coherently scattering domain (CSD) size using the Scherrer equation (eq 1)

$$D = (K \cdot \lambda) / (\beta \cos \theta) \quad (1)$$

K is the shape factor = 0.9, β_{inst} is the instrumental line broadening = 0.07°.

Nitrogen multipoint adsorption/desorption isotherms at –196 °C (77 K) were collected using Micromeritics ASAP 2020 and Micromeritics ASAP 2420 instruments.

The total acidity and basicity of catalysts were measured by means of the temperature-programmed desorption (TPD) of NH₃ and CO₂ using a Micromeritics AutoChem II 2920 instrument. Effluents were analyzed using a Cirrus 2 quadrupole mass spectrometer recording the intensity of the following ion current signals: NH₃ ($m/z = 17$), H₂O ($m/z = 18$), CO₂ ($m/z = 44$).

Typically, 0.2 g of samples was charged in a quartz tube and heated up to calcination temperature in a He flow (30 mL/min) with a heating rate of 10 °C/min. The final temperature was kept for 60 min to clean the adsorbed water and carbonates from the catalyst surface. After cooling, NH₃ and CO₂ chemisorption studies were conducted at 100 °C for 20 min of flowing 10% NH₃/He (30 mL/min) and 40 °C for 60 min of flowing 10% CO₂/He (30 mL/min), respectively. Before desorption, samples were flowed with He (30 mL/min) for 60 min at the adsorption temperature to remove the weakly physisorbed probe molecules.

Last, temperature-programmed desorption (TPD) was conducted in the same way as for the sample surface cleaning.

Thermogravimetric analyses (TGA) of catalysts after the reaction were performed with an SDTQ 600 instrument. Typically, 15 mg of samples was loaded into an alumina pan and heated up to 600 °C with a heating rate of 10 °C/min in 100 mL/min of N₂; the final temperature was kept for 1 h. Then, the gaseous flow was switched from N₂ to air to burn all carbonaceous deposits on the catalyst surface; the final temperature was kept for 1 h.

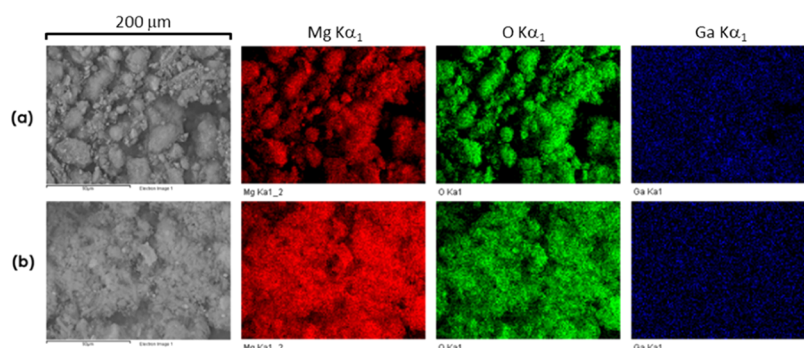
X-ray photoelectron spectroscopy (XPS) spectra were recorded with a PHI VersaProbe II scanning XPS microprobe with a scanning monochromatic X-ray Al K α radiation as the excitation source (200 μm , 52.8 W, 15 kV, 1486.6 eV) and a charge neutralizer. The analysis chamber pressure was maintained lower than 2.0×10^{-6} Pa. High-resolution spectra were recorded at a given 45° takeoff angle by a multichannel hemispherical electron analyzer operating in the constant pass energy mode at 29.35 eV. The energy scale was calibrated using Cu 2p_{3/2}, Ag 3d_{5/2}, and Au 4f_{7/2} photoelectron lines at 932.6, 368.2, and 83.9 eV, respectively.

Scanning electron microscopy (SEM)-energy-dispersive spectrometry (EDS) images were recorded using an EVO50 series instrument (LEO ZEISS) equipped with an INCAEnergy350 EDS microanalysis

Table 1. Physicochemical Properties of Fresh Catalysts^a

catalyst	BET-SSA (m ² /g)	CSD size (nm)	total basicity (μmol/(m ² ·CO ₂))	total acidity (μmol/(m ² ·NH ₃))	atomic Mg/Ga ratio ^a
MgO	181	9.4	3.53	0.09	∞
Mg/Ga-20	118	9.3	2.54	0.41	21.4
Mg/Ga-10	132	11.2	1.26	1.13	9.8
Ga ₂ O ₃	14	37.1	0.41	3.86	

^aThe Mg/Ga atomic ratio was determined by semi-quantitative SEM-EDS analysis, and the values are in good agreement with the XPS characterization of these materials.

**Figure 1.** SEM electron images and EDS elemental maps of (a) Mg/Ga-10 and (b) Mg/Ga-20.

system and INCASmartMap (Oxford Instruments Analytical) for the elemental mapping of elements and the determination of Mg/Ga ratios. The accelerating voltage was 20 kV, and the spectra were recorded in a duration of 60 s.

Catalytic Tests. All catalytic tests were performed at atmospheric pressure by loading catalyst pellets (particle size = 30–60 mesh) into the isotherm section of a conventional fixed-bed down-flow quartz reactor. MP (Alfa Aesar, 99%) and MeOH (Sigma-Aldrich, 99.9%) were mixed in the desired molar ratio, and the feed liquid mixture was injected by means of a volumetric pump (KD Scientific Legacy 100) in a stainless steel line (1/16 in.) and driven directly 5 cm above the catalytic bed with 12 mL/min of N₂. A second flux of preheated N₂ (210 °C) was driven to the head of the reactor from another stainless steel line (1/8 in.) to obtain the desired total N₂ flux.

Except when otherwise specified, the charged catalyst mass was 1.15 g, the total volumetric flow of gaseous (MP + MeOH + N₂) at 25 °C was 65 mL/min, and the composition (mol %) MP/MeOH/N₂ was 1/5/94; the resulting time factor (catalyst weight divided by the total volumetric flow at the reaction temperature, W/F) calculated at 350 °C was equal to 0.5 s·g/mL. To maintain the same W/F, when changing the reaction temperature, both N₂ and the liquid mixture flow rate were increased or reduced accordingly. The effect of W/F at constant temperature was investigated while keeping the same total flow rate and increasing or reducing the catalyst mass. Usually, the catalyst was heated up to reaction temperature at 10 °C/min under a nitrogen flow (the same flow that will be used to carry out the catalytic test) and then kept at this temperature for 30 min before starting to feed the reactant mixture.

Liquid products were absorbed in absolute ethanol (EtOH, Sigma-Aldrich, 99.8%) or acetonitrile (AcCN, Sigma-Aldrich, 99.8%), bubbling the outlet from the reactor in three cold traps in series, maintained at 0 °C with an ice bath. The products and unconverted reactant were transferred from the cold traps to a 100 mL flask at regular time intervals, while 1 g of dodecane (Sigma-Aldrich, 99%) solution (4 × 10⁻⁵ mol/g) was added as the internal standard.

Gaseous products leaving the cold trap were driven into an online gas chromatography (GC) equipped with two sample/injection loops in series. Both the liquid reaction mixtures and gases exiting from the cold trap were analyzed by gas chromatography with a Hewlett Packard 5890 series II GC instrument equipped with flame ionization detector (FID) and thermal conductivity detector (TCD). An Agilent J&W DB-1701 capillary column (25 m × 530 μm × 1.05 μm) connected to the FID was used for the offline quantification of the

condensed products. For the online quantification of gaseous products, an Agilent CP-Molsieve 5 Å capillary column (25 m × 530 μm × 50 μm, to elute H₂, O₂ and N₂) and an Agilent CP-SilicaPLOT capillary column (30 m × 530 μm × 6 μm, to elute CO, CO₂, CH₄, ethylene, propylene, and propane) were used.

Unknown products were identified by means of GC-MS with an Agilent Technologies 6890 gas chromatographer equipped with an Agilent HP-5 capillary column (30 m × 250 μm × 1.05 μm and an Agilent Technologies 5973 mass analyzer), and the retention time of unknown products was compared with that of pure reference standards.

All catalytic tests were performed for at least 6 h and results were calculated once the system had reached a stationary state; most experiments were also triplicated to check for reproducibility, and, in the repeated runs carried out under the same conditions, the values of conversion and yields differed by less than 5% from one reaction to another.

Two “blank” tests were also performed to assess the stability of both the reactants (MP and MeOH) and the product (MMA) when fed into the reactor in the absence of catalytic materials; results are shown in Figures S1 and S2.

Conversion (X_{MP}), yields (Y_i), selectivities (S_i), the sum of yields (yield sum), and molar balance (yield sum/ X_{MP}) were calculated according to the following equations

$$X_{MP} = [(\text{mol}_{MPIN} - \text{mol}_{MPOUT}) / (\text{mol}_{MPIN})] \times 100 \quad (2)$$

$$Y_i = \nu \cdot (\text{mol}_{out} / \text{mol}_{MPIN}) \times 100 \quad (\nu: \text{stoichiometric coefficient}) \quad (3)$$

$$S_i = (Y_i / X_{MP}) \times 100 \quad (4)$$

$$\text{yield sum} = \sum_i Y_i \quad (5)$$

$$\text{molar balance} = \text{yield sum} / X_{MP} = \left(\sum_i Y_i \right) / X_{MP} \times 100 \quad (6)$$

RESULTS AND DISCUSSION

Characterization of Fresh Catalysts. The main features of the catalysts are summarized in Table 1. All synthesized catalysts (MgO, Mg/Ga-20, and Mg/Ga-10) had surface areas

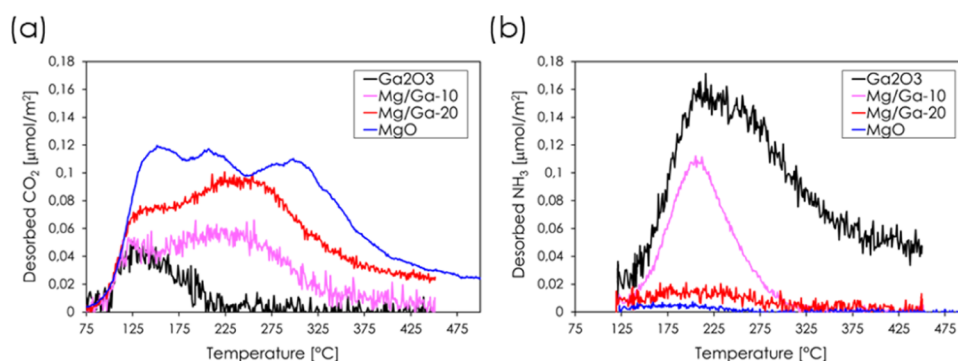


Figure 2. (a) CO₂-TPD and (b) NH₃-TPD profiles for Ga₂O₃, Mg/Ga-10, Mg/Ga-20, and MgO.

higher than 100 m²/g, while the commercial Ga₂O₃ was characterized by a relatively low surface area of 14 m²/g.

The XRD patterns of the catalysts are shown in Figure S3 (see the Supporting Information). Commercial Ga₂O₃ (Figure S3a) showed the typical reflections of the most stable monoclinic β -phase (PDF number 01-076-0573). Synthesized MgO, Mg/Ga-10 and Mg/Ga-20 XRD patterns (Figure S3c–e, respectively) were characterized by reflection lines in very good agreement with the periclase structure of MgO (PDF number 01-089-7746), without any impurities such as Ga₂O₃ polymorphs or the spinel-phase MgGa₂O₄.

The average crystallite sizes (CSD) were calculated using the Scherrer equation (eq 1), and the relevant values are shown in Table 1. Results indicate that commercial Ga₂O₃ had a larger crystallite size and was more crystalline than all of the other catalysts.

Figure 1 shows, from left to right, the SEM electron image and the EDS elemental maps of magnesium (red), oxygen (yellow), and gallium (blue) for the mixed metal oxides Mg/Ga-10 (a) and Mg/Ga-20 (b); in both cases, Ga is homogeneously distributed all over the sample. The results of both XRD and SEM-EDS analyses indicate that Mg/Ga-10 and Mg/Ga-20 are true mixed metal solid solutions obtained by the partial substitution of Mg²⁺ ions with Ga³⁺ ions.

On the other hand, the XRD pattern of a physical mixture of MgO and β -Ga₂O₃ (Mg/Ga-mix, Figure S3b) exhibited a first set of broad diffraction peaks attributable to the presence of MgO ($2\theta = 37, 43, 63, 75,$ and 79° , indicated by black dotted lines in Figure S3), while all other diffraction peaks were sharper and attributable to the presence of β -Ga₂O₃; in other words, the XRD pattern of the physical mixture arose from the combination of the patterns of MgO and β -Ga₂O₃.

The CO₂-TPD profiles of Ga₂O₃, Mg/Ga-20, Mg/Ga-10, and MgO are shown in Figure 2a. In agreement with recent literature,³³ the desorption profile for MgO (in blue) displayed three peaks at around 150, 210, and 300 °C; however, CO₂ kept desorbing even at higher temperatures (up to 500 °C) and stopped only during the final isotherm.

The three desorption peaks arise from the presence of basic sites with different strengths. Basic sites in MgO consist of O²⁻ anions bound to highly electropositive Mg²⁺ cations; O²⁻ anions, which occupy increasingly defective positions (terraces < edges < corners < O²⁻ anions neighboring cationic holes), display a stronger basicity due to their increasing lack of coordination.

According to the literature, in MgO-based mixed systems containing a more electronegative guest cation such as Ga³⁺, both the density and the strength of basic sites decrease

compared to pure MgO due to the higher covalent character of the Ga–O bond.³⁴

This behavior can be seen in TPD profiles of Mg/Ga-20 (in red) and Mg/Ga-10 (in magenta), where the strength and density of basic sites decreased with an increase in the Ga³⁺ content. Mg/Ga-20 showed two peaks at 140 and 245 °C, then carbon dioxide release continued up to the calcination temperature and stopped during the final isothermal step. The CO₂-TPD of Mg/Ga-10 showed a similar profile, with a lower density of basic sites and two peaks at 135 and 220 °C. In this case, CO₂ desorption approaching calcination temperature was very low, indicating that in this catalyst there is a much lower concentration of the strongest basic sites present in Mg/Ga-20 and MgO.

Last, the CO₂-TPD profile of Ga₂O₃ (in black) showed only one desorption peak centered in the low temperature range corresponding to weak basic sites, while CO₂ desorption stopped completely at around 210 °C.

The NH₃-TPD profiles for Ga₂O₃, Mg/Ga-20, Mg/Ga-10, and MgO are shown in Figure 2b. As expected, MgO (in blue) and Mg/Ga-20 (in red) desorbed very small amounts of NH₃ (0.09 and 0.41 $\mu\text{mol}/\text{m}^2$, respectively) in a broad temperature range centered around 190 and 205 °C, respectively; these two materials were the ones possessing the weakest and fewest acidic sites.

Mg/Ga-10 (in magenta) showed a much higher density (1.13 $\mu\text{mol}/\text{m}^2$ of NH₃) of acidic sites compared to MgO and Mg/Ga-20, with a desorption peak at 210 °C. Last, Ga₂O₃ (in black) displayed the highest density of acidic sites (3.86 $\mu\text{mol}/\text{m}^2$ of NH₃), with a peak centered at 215 °C.

NH₃, however, kept desorbing from the Ga₂O₃ surface up to calcination temperature (450 °C) and stopped only during the final isothermal step, thus suggesting the presence of a significant fraction of strong acidic sites in this material.

To summarize, increasing the Ga content in Mg/Ga mixed metal oxide solutions modulates catalyst basicity by reducing the strength and the density of basic sites compared to pure MgO; on the other hand, the density and strength of acidic sites were increased significantly only when the Mg/Ga ratio in the mixed oxide was equal to 10.

Last, the two pure oxides MgO and Ga₂O₃ have the strongest basic and acidic sites, respectively, among all of the materials investigated.

Catalytic Activity of MgO and the Determination of a Complex Reaction Network. MgO was chosen as the reference catalyst to investigate the “one-pot” synthesis of MMA from MP and FAL produced *in situ* because of its well-known dehydrogenative properties toward MeOH at high

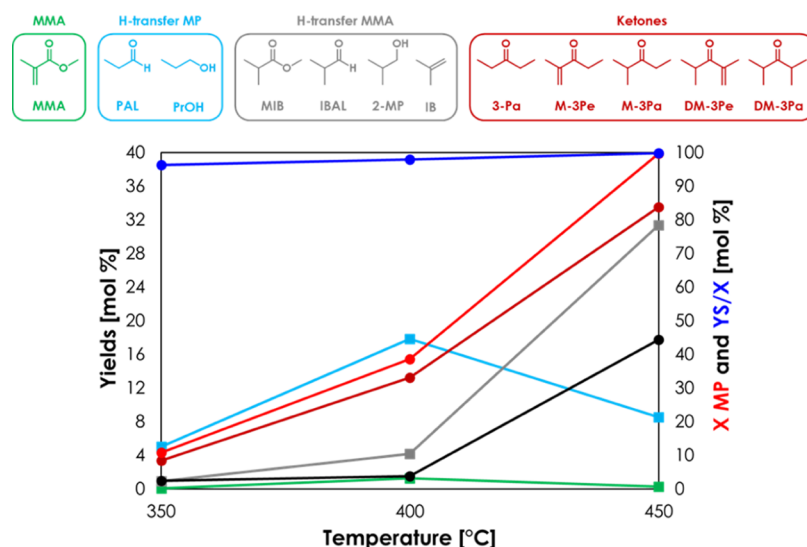
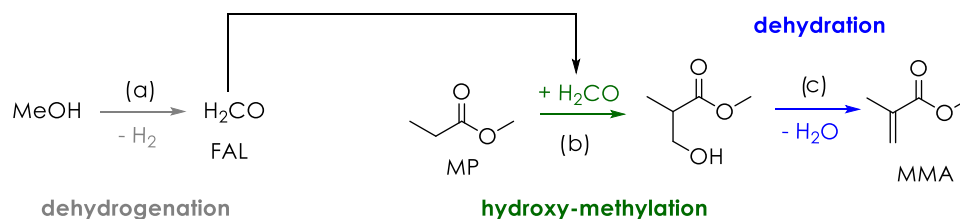


Figure 3. Catalytic activity of MgO. Reaction conditions: feed composition (mol %) MP/MeOH/N₂ = 1/5/94; W/F (time factor) = 0.5 s·g/mL. Right y-axis: MP conversion (X MP) and molar balance (YS/X). Left y-axis: yields. Symbols: X MP (red solid circle), YS/X (blue solid circle), MMA (green solid square), the sum of yields of H-transfer products from MP (light blue solid square), the sum of yields of H-transfer products from MMA (gray solid square), the sum of yields of ketones (dark red solid circle), and others (black solid circle). “Others” includes propionic acid (PA), methacrylic acid (MAA), and unknown compounds.

Scheme 2. Proposed Reaction Pathway for MMA Synthesis



temperatures,^{27,28} which led to its frequent use as a benchmark for basic-catalyzed reactions.^{33–36}

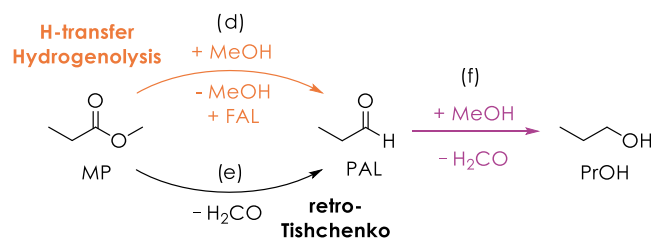
The outstream reaction mixtures were characterized by a high number of products; however, their formation is ultimately attributable to four main reaction pathways contributing to the overall reaction scheme.

Therefore, it was decided to classify the products into the four categories shown in Figure 3 and to report the results obtained on MgO at 350, 400, and 450 °C with a constant time factor (W/F = 0.5 s·g/mL) and gaseous feed composition (MP/MeOH/N₂ = 1/5/94 mol %) in terms of the sum of the yields of the products in each category, to simplify the interpretation of graphs and clarify the main reaction pathways.

The first category of products (in green in Figure 3) consists of MMA alone, which is formed by the reactions depicted in Scheme 2: MeOH dehydrogenation to FAL *in situ* (a), hydroxymethylation of MP with FAL (b), and consecutive dehydration of the resulting hydroxymethyl intermediate (c).

The second group of products (in light blue in Figure 3), named “H-transfer MP”, consists of propionaldehyde (PAL) and 1-propanol (PrOH), and the proposed reaction pathway for their formation is depicted in Scheme 3. In these molecules the alkyl moiety is unchanged with respect to MP; therefore, their formation from MMA can be ruled out. Instead, PAL may be formed via either retro-Tishchenko pathway³⁷ (e) or H-transfer hydrogenolysis of the C–O bond of MP with MeOH or FAL as H-donors (d); a consecutive H-transfer hydrogenation of the carbonyl group of PAL results in the formation

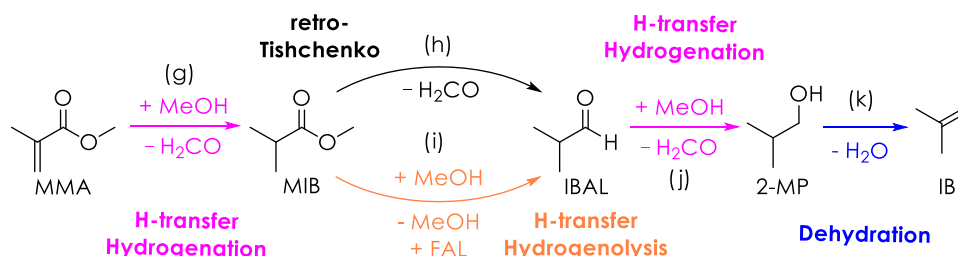
Scheme 3. Proposed Reaction Leading to H-Transfer MP ByProducts



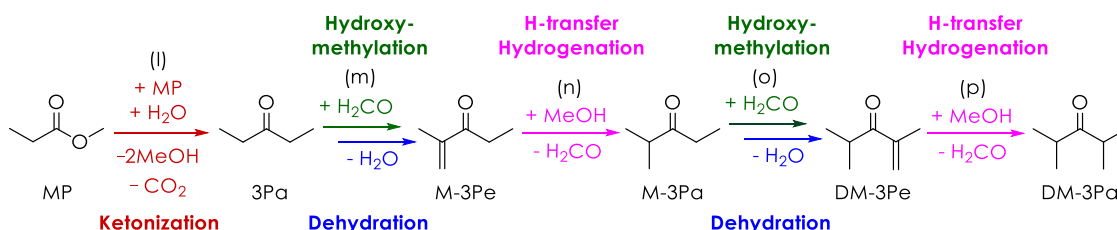
of PrOH (f).³⁸ The distribution of these products is shown in Figure S4.

The third group of products (in gray in Figure 3) is composed of methyl isobutyrate (MIB), isobutyraldehyde (IBAL), 2-methyl propanol (2-MP), and isobutylene (IB). All of these molecules share a 4-carbon atom alkyl moiety branched in the α -position as MMA does; therefore, their formation is attributable to consecutive reactions occurring on the target product, and the proposed reaction pathway for their formation is depicted in Scheme 4. In particular, MIB may be formed by H-transfer hydrogenation of the C=C double bond of MMA (g),^{30,31} IBAL is formed by either MIB retro-Tishchenko pathway³⁷ (h) or H-transfer hydrogenolysis (i), and 2-MP is formed by the H-transfer hydrogenation of the C=O double bond of IBAL (j).^{38,39} Last, IB is the product of 2-MP dehydration (k).⁴⁰

Scheme 4. Proposed Reaction Pathway Leading to H-Transfer MMA ByProducts



Scheme 5. Proposed Reaction Pathway Leading to Ketones ByProducts



This group of products will be called “H-transfer MMA”, and their product distribution is shown in Figure S5. The occurrence of H-transfer parasitic reactions is a consequence of the mechanism of MeOH dehydrogenation on MgO, which is known to require (1) MeOH dissociation into a proton and a methoxide ion on the catalyst surface and (2) a hydride (H^-) transfer from the methoxide ion to the proton, resulting in the formation of FAL and H_2 .²⁸ However, when other compounds (e.g., MP, PAL, and MMA) are present on the catalyst surface, their C–O, C=O, and C=C functionalities can act as hydride acceptors, resulting in H-transfer hydrogenations, which are known to occur on MgO.^{41–43}

The fourth group of products (in dark red in Figure 3) will be referred to as “ketones” and consists of 3-pentanone (3Pa), 2-methyl-3-pentenone (M-3Pe), 2-methyl-3-pentanone (M-3Pa), 2,4-dimethyl-3-pentenone (DM-3Pe), and 2,4-dimethyl-3-pentanone (DM-3Pa). In these molecules, the main alkyl chain consists of five carbon atoms, plus a variable number of side-chain methyl ($-\text{CH}_3$) or methylenes ($=\text{CH}_2$) groups. Ketonization occurs when MP, after an activation via α -hydrogen abstraction, reacts with another MP molecule and a molecule of water, producing 3Pa, CO_2 , and two molecules of MeOH.⁴⁴ The other compounds of this group are formed by consecutive hydroxymethylations/dehydrations (m, o) and H-transfer hydrogenations (n, p) occurring on 3Pa (e.g., M-3Pe from hydroxymethylation and dehydration (m) of 3Pa and M-3Pa from H-transfer hydrogenation (n) of the methylenes group of M-3Pe). The yield in CO_2 was very similar to the sum of yields of all ketones below 400 °C, indicating that it is formed only by the ketonization reaction. Above this temperature, the yield in CO_2 became higher than the one in ketones, suggesting a contribution of MeOH/FAL decomposition. A detailed distribution of the obtained ketones and CO_2 is shown in Figure S6, and the proposed reaction pathway leading to ketones is depicted in Scheme 5.

As can be seen in Figure 3, between 350 and 400 °C, MgO leads to a moderate conversion of MP (11 and 39%, respectively), triggering the formation of both H-transfer MP products (5 and 19% yields) and ketones (3.5 and 13% yields); however, the MMA yield was very low (0 and 1.3%). Interestingly, at high temperature, 450 °C, MP conversion

increased to 100%, and both H-transfer MMA compounds and ketones became the main products, obtained with similar yields (31 and 32%, respectively). These results suggest that MMA is not obtained in the lower temperature range (350–400 °C) because in these conditions MgO has weak dehydrogenative activity toward MeOH, and the resulting FAL is not sufficient for MP hydroxymethylation to compete with the side reaction of ketonization and H-transfer. Instead, at 450 °C, MgO becomes much more active for MeOH dehydrogenation and provides enough FAL for hydroxymethylations of both MP and 3Pa to occur extensively (Figures S5 and S6, respectively). However, higher temperatures also trigger consecutive H-transfer hydrogenations of MMA, which is immediately transformed into other compounds.

The feed composition has a dramatic effect on the extent of these side reactions. As a matter of fact, when the concentration of MP was increased by limiting MeOH excess (feed composition MP/MeOH/ N_2 = 6/12/82 mol %, Figure S7), the bimolecular ketonization of MP became the main reaction pathway in the low temperature range (350–450 °C) at the expense of both hydroxymethylation and H-transfer reduction.

Only at a very high temperature (500 °C), FAL is formed in large amounts to promote the formation of MMA, which, however, is further reduced by H-transfer hydrogenation (Figure S8).

The ketone distribution in the latter conditions (Figure S9) confirms the proposed pathway for their formation. 3Pa is the main product in the low temperature range due to the scarce dehydrogenating activity of MgO and, as a consequence, low activity for hydroxymethylation of 3Pa. In fact, by raising the temperature from 350 to 400 °C, 3Pa yield increases from 1.8 to 6.0%, finally reaching 25.9% at 450 °C. A further increase in the reaction temperature up to 500 °C led to a drop in the yield of 3Pa down to 9.8% because it is consumed to produce M-3Pe by hydroxymethylation. The yield of M-3Pe shows a similar trend: it increases when the reaction temperature is raised up to 450 °C (7.7%) but then drops to 500 °C (3.5%) because it is consumed to produce M-3Pa by H-transfer hydrogenation.

Effect of a Strong Redox Character on Catalytic Activity: Ga₂O₃. The results obtained on MgO suggest that a strong dehydrogenating activity is desirable to promote the formation of a large excess of FAL with respect to MP at lower temperatures, thus limiting both ketonization and H-transfer, which are triggered by high temperatures. Starting from this hypothesis, it was decided to compare the catalytic activity of MgO with that of Ga₂O₃, which has a much stronger dehydrogenating activity^{45–47} and a lower activity toward ketonization.⁴⁸

The results obtained with Ga₂O₃ are shown in Figure 4.

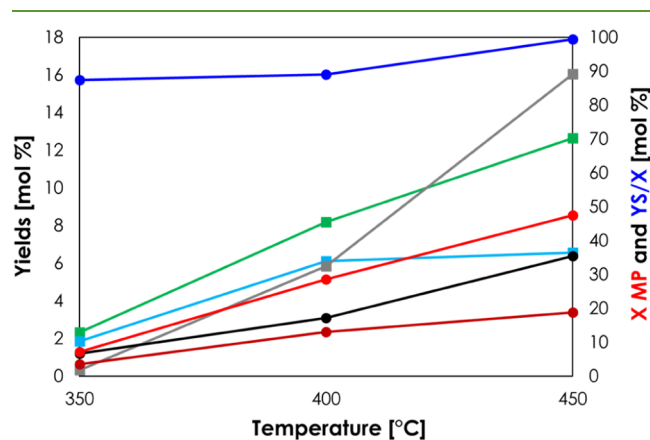


Figure 4. Catalytic activity of Ga₂O₃. Reaction conditions: feed composition (mol %) MP/MeOH/N₂ = 1/5/94; W/F (time factor) = 0.5 s·g/mL. Right-y-axis: MP conversion (X MP) and molar balance (YS/X). Left-y-axis: yields. Symbols: X MP (red solid circle), YS/X (blue solid circle), MMA (green solid square), sum of yields of H-transfer products from MP (light blue solid square), sum of yields of H-transfer products from MMA (gray solid square), sum of yields of ketones (dark red solid circle), others (black solid square). “Others” includes propionic acid (PA), methacrylic acid (MAA), propylene, and unknown compounds. MeOH conversion = 21.8% (350 °C), 32.2% (400 °C) and 56.2% (450 °C); MMA selectivity in respect to MeOH = 2.2% (352 °C), 4.9% (400 °C) and 4.5% (450 °C).

As expected, MP conversion progressively increased with increasing reaction temperature from 7% (350 °C) to 47.5% (450 °C), with good-to-excellent molar balance (from 90 to 100%). Thanks to its higher redox activity, Ga₂O₃ dehydrogenates MeOH to FAL at much lower temperatures with respect to MgO, thus fostering the hydroxymethylation/dehydration pathway of MP.

Worthy of note, MMA was the main product in all of the temperature ranges investigated (2, 8, and 13% yields at 350, 400, and 450 °C, respectively), while ketonization, far from being a significant side reaction as with MgO, yielded only 3.5% of ketones at 450 °C.

Instead, on this catalyst, the major byproducts were reduced compounds (e.g., PAL, MIB, MAL, and IBAL) deriving from H-transfer reactions, which preferentially consumed MP at 350 °C, both MP and MMA at 400 °C, and mainly MMA at 450 °C.

Even if H-transfer hydrogenations were triggered on both MgO and Ga₂O₃ by raising the reaction temperature, the degree of hydrogenation of H-transfer MMA products obtained on MgO was higher than that obtained on Ga₂O₃ under similar conditions, thus indicating that the latter catalyst is intrinsically less active for H-transfer reactions. As an example, on Ga₂O₃, the H-transfer MMA products at 450 °C

were methacrolein (MAL, yield = 4%), MIB (7%), and IBAL (4.8%); their distribution is shown in Figure S10. Instead, on MgO, MAL was absent and MIB yield was only 2%, while significant amounts of IBAL (7.5%), 2-MP (18.5%), and IB (10.9%) were obtained (Figure S5).

The formation of MAL can be explained by the H-transfer hydrogenolysis of the C–O bond of MMA, by the retro-Tishchenko pathway of MMA, or by the hydroxymethylation and dehydration of PAL. Even if all of these three pathways are theoretically possible, it is likely that certain reaction conditions may be more favorable to one than to the others (e.g., the MMA retro-Tishchenko pathway may be triggered by the absence of H-donors, while the other two pathways may be induced by MeOH/FAL-rich environments).

To clarify this aspect, it was attempted to demonstrate the occurrence of the retro-Tishchenko pathway by feeding MMA or MP onto Ga₂O₃ in the absence of MeOH in the feed at 450 °C. The results in Figure S11 show that MMA does not react on Ga₂O₃ and MAL is not obtained in the absence of MeOH in the feed, thus suggesting that the retro-Tishchenko pathway does not occur. When MP was fed onto Ga₂O₃ under the same reaction conditions, a much higher conversion (70%) was achieved, and both PAL and 3Pa were obtained. However, MP ketonization co-produces 2 mol of MeOH for each mole of 3Pa; therefore, in this case, the formation of PAL via the MP hydrogenolysis pathway cannot be completely ruled out even if MeOH was absent from the feed. Finally, IBAL may also be formed from MAL by means of the H-transfer hydrogenation of the C=C double bond of the latter.³⁹

The results shown in Figures 3 and 4 were obtained by calculating the average value of conversion and the yields obtained after conducting a catalytic test with MgO and Ga₂O₃ at each temperature for at least 6 h. In all cases, the catalysts did not deactivate in such a short reaction time, with the sole exception of Ga₂O₃ at 450 °C, where both MP conversion and product yields decreased steadily with an increase of the time on stream (Figure S12). Therefore, the deactivation of Ga₂O₃ was further investigated by repeating the catalytic test with a fresh portion of catalyst for a longer reaction time. Then, we investigated its regeneration *in situ* by feeding air and its performance when the catalytic test was repeated in the same reaction conditions after regeneration (Figure 5).

During an 18 h time-on-stream test, MP conversion on the fresh catalyst (Ga₂O₃) dropped from 72% down to 19%, indicating that most of the active sites on the catalyst surface were progressively deactivated. Despite the extensive occurrence of H-transfer hydrogenation of MMA during the first 3 h of the reaction, over the next 9 h, the yields of byproducts decreased to values well below 5%, with the exception of only the H-transfer MP products; at the same time, MMA became the major product and its yield stabilized at around 12.5%. Last, starting from the 12th hour of the reaction, MMA yield also started to decrease, dropping to 7% at the 18th hour of the reaction. A detailed distribution for H-transfer MMA products during this experiment can be found in the Supporting Information (Figure S13). The greater activity of the catalyst during the first hours of the reaction was accompanied by a lower molar balance (80%) and higher yields toward side products; however, as deactivation proceeded and MP conversion was reduced, the molar balance improved, growing close to 100%.

Such behavior can be explained by the occurrence of consecutive side reactions such as FAL polymerization and

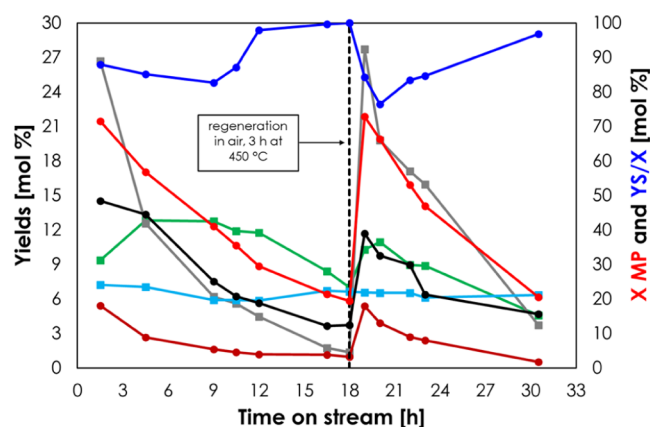


Figure 5. Catalytic activity of Ga_2O_3 . Reaction conditions: feed composition (mol %) MP/MeOH/ N_2 = 1/5/94; W/F (time factor) = 0.5 s-g/mL; temperature = 450 °C. Right y-axis: MP conversion (X_{MP}) and molar balance ($Y_{\text{S/X}}$). Left y-axis: yields. Symbols: X_{MP} (red solid circle), $Y_{\text{S/X}}$ (blue solid circle), MMA (green solid square), the sum of yields of H-transfer products from MP (light blue solid square), the sum of yields of H-transfer products from MMA (gray solid square), the sum of yields of ketones (dark red solid circle), and others (black solid circle). “Others” includes propionic acid (PA), methacrylic acid (MAA), propylene, and unknown compounds.

aldol condensations of ketones occurring on the most active sites (e.g., strong acidic sites) during the first 12 h of the reaction; MMA homo-polymerization was ruled out on the basis of its very low reactivity on Ga_2O_3 shown in Figure S11. The progressive deactivation due to fouling of the acidic sites led, after several hours of the reaction, to a lower MP conversion, better molar balance, and higher MMA selectivity. It is worth noting that the aforementioned side/consecutive reactions also led to the formation of heavy compounds, which were able to desorb from the catalyst surface but then condensed in the relatively colder zone below the catalytic bed, leaving a brown residue on the reactor walls, which could not be collected during the sampling and contributed to the deficit in the molar balance; an image of these carbon residues is shown in Figure S14.

Simple regeneration with a 20 mL/min air flow at 450 °C for 3 h restored MP conversion back to its initial value (73%) with minor changes in product selectivity; however, compared to the fresh catalyst, the conversion dropped to 20% within a shorter reaction time period (12 h), indicating that the deactivation of the recycled catalyst was faster than the one of the fresh catalyst.

To investigate the reasons behind the catalyst deactivation, Ga_2O_3 was characterized by means of TGA, XRD, XPS, and N_2 porosimetry after the first 18 h of the reaction and before regeneration and recycling. The main results of these measurements are summarized in Table 2.

The loss of the specific surface area of the catalyst after the reaction, even if limited, amounts to 57% of the initial SSA of the fresh catalyst; therefore, it should be considered significant and is probably the main reason for the catalyst's loss of activity.

Diffraction patterns before (a) and after the reaction (b) are shown in Figure S15. The crystal structure of Ga_2O_3 was retained without any significant difference in peak positions, broadness, and intensity; moreover, the CSD sizes calculated from the Scherrer equation (eq 1) before and after the reaction

Table 2. Ga_2O_3 Physicochemical Properties before and after the Reaction

Ga_2O_3	BET-SSA ^a (m ² /g)	crystal phase ^b	TGA mass loss (%)	surface carbon (XPS) (mol %)
fresh	14 ^c	β		12.6 ^e
after the reaction	6 ^d	β	1.05	52.3

^aNitrogen porosimetry. ^bXRD. ^cTGA. ^dXPS. ^eAdventitious carbon.

(37.1 and 36.7 nm, respectively) were practically unchanged. Therefore, the loss of the specific surface area is not attributable to changes in its crystal structure, such as the formation of a different polymorph.

The mass loss measured by means of TGA was very low (Table 2 and Figure S16) and did not explain the deficit in the molar balance, which was observed during the reaction; therefore, it was concluded that this deficit is mainly attributable to the formation, at the beginning of the reaction, of heavy products, which condensed on reactor walls.

X-ray photoelectron spectroscopy was used to investigate the catalyst surface, and XPS survey spectra for Ga_2O_3 , before and after the reaction, can be found in the Supporting Information, Figures S17 and S18, respectively.

Figure 6 shows the XPS high-resolution spectra of the C 1s core level for Ga_2O_3 before (a) and after (b) the reaction. In

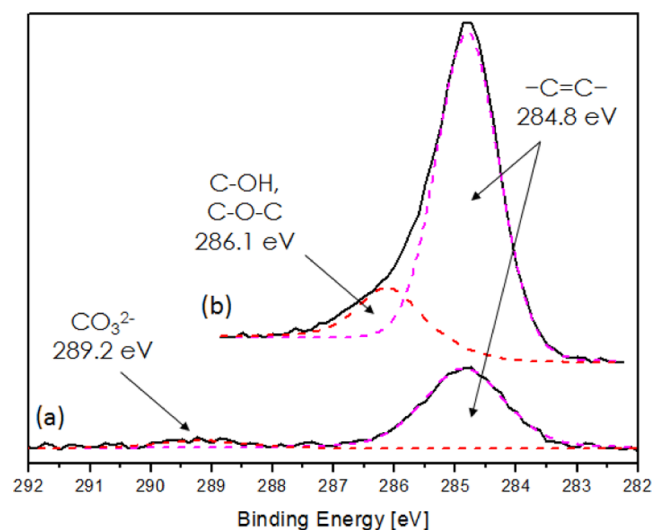


Figure 6. XPS high-resolution C 1s core-level spectra of (a) Ga_2O_3 fresh and (b) Ga_2O_3 after 18 h of the reaction.

the fresh catalyst, roughly 13% of surface atoms were carbons, present both as adventitious graphitic carbon (284.8 eV) and in the form of carbonate species (289.2 eV).⁴⁹ After the reaction, carbon alone represented more than 52% of the surface atoms; the intensity of the graphitic carbon peak was significantly higher, while the carbonate peak disappeared, with the appearance of a new signal centered at 286.1 eV, which can be attributed to the presence of polymers containing C–O bonds.⁴⁹

The XPS spectra of the O 1s core level for Ga_2O_3 before (a) and after (b) the reaction are shown in Figure S19; in both cases, two signals centered at 530.8 and 532.2 eV were observed. The former was attributed to O^{2-} bonded to Ga^{3+} (ref 531.2 eV),⁵⁰ while the latter may result from the presence of organic molecules containing C–O bonds (ref 532.2 eV).⁵¹

Last, Figure S20 shows the XPS spectrum of the Ga 2p_{3/2} core level for Ga₂O₃ before (a) and after (b) reaction: in both cases, all Ga was present entirely as Ga³⁺ (1118.0–1118.1 eV);^{50,52} therefore, it may be concluded that surface Ga³⁺ was not reduced under reaction conditions and that catalyst deactivation did not depend on the formation of superficial Ga(0) species (ref 1116.6 eV).⁵²

The experimental surface Ga/O atomic ratio for fresh Ga₂O₃, calculated from XPS spectra, was 0.664, which is in good agreement with the theoretical value of 0.666. Conversely, in the case of the spent catalyst, the Ga/O atomic ratio (0.420) was lower than the theoretical one due to the presence of oxygen-containing organic molecules.

In conclusion, the result of the XPS-electron spectroscopy for chemical analysis (ESCA) semiquantitative elemental analysis suggests that, during the reaction, the surface of the catalyst was progressively covered by carbon residues, possibly blocking pores and leading to a significant reduction in the surface area available to the reactants, thus causing catalyst deactivation. Considering the very low (14 m²/g) specific surface area of fresh Ga₂O₃, it is possible that small amounts of carbon residues are sufficient to cause deactivation, thus explaining the very low weight loss measured by TGA. Last, since MgO did not deactivate during the time on stream at 450 °C (Figure S21), it can be concluded that the deactivation of Ga₂O₃ is likely attributable to the presence of strong acidic sites on its surface, which, instead, are absent on MgO.

Role of Ga as a Redox Promoter in Mg/Ga Mixed Oxide Solutions. The use of Ga in the formulation of a catalyst to be used in a large-scale production is affected by two major issues: its cost and its availability. In fact, the only profitable process for obtaining Ga is its extraction from bauxite (where it is found in traces) during aluminium production and therefore, even if it is not rare,⁵³ the world supply of Ga is limited to 10²–10³ t/year because it is linked to the Al demand.⁵⁴ Moreover, it is considered a technology-critical element⁵⁴ with applications in several strategic high-tech products. Therefore, it is advisable to reduce as much as possible the Ga content in the formulation of a catalyst for MMA production, in view of a hypothetical scale-up of the process.

Since the incorporation of redox guest cations into MgO-based mixed oxides is known to boost their dehydrogenating activity and sensibly reduce the temperature needed to obtain FAL from MeOH,^{29,45,55} it was decided to evaluate Ga³⁺ as a dehydrogenation promoter in MgO-based mixed oxides as a strategy to reduce the Ga content in a catalyst formulation. As a proof of concept, two mixed metal oxides containing a small fraction of Ga³⁺ ions were prepared (Mg/Ga atomic ratios equal to 10 and 20), and their performances were evaluated at 400 °C, W/F = 0.5 s·g/mL with a gaseous feed composition MP/MeOH/N₂ = 1/5/94 mol %.

Figure 7 shows the comparison between the catalytic activity of the prepared mixed oxides and that of the two single metal oxides, as well as that of a physical mixture of MgO and Ga₂O₃ (Mg/Ga atomic ratio = 10); results obtained with a 5 wt % Cs/SiO₂ catalyst in the same conditions are also included in Figure 7 to provide a comparison with the Lucite Alpha process catalyst (detailed information regarding its synthesis can be found in the Supporting Information, p S22). Remarkably, the Cs/SiO₂ catalyst was the least active for the target reactions: in fact, being designed to produce MMA from a feed consisting of FAL/MP and not MeOH/MP, it lacks the

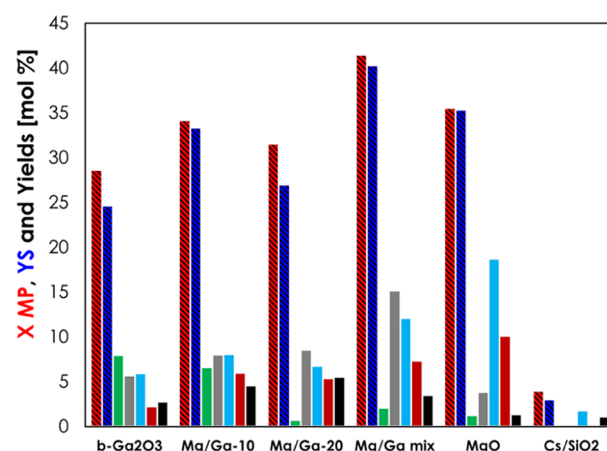


Figure 7. Catalytic activity of Ga₂O₃, Mg/Ga-10, Mg/Ga-20, Mg/Ga-mix, MgO, and 5% Cs/SiO₂. Reaction conditions: feed composition (mol %) MP/MeOH/N₂ = 1/5/94; W/F (time factor) = 0.5 s·g/mL; temperature = 400 °C. Symbols: X MP (red bar), YS (blue bar), MMA (green bar), sum of the yields of H-transfer products from MP (light blue bar), sum of the yields of H-transfer products from MMA (gray bar), sum of the yields of ketones (dark red bar), and others (black bar). “Others” includes propionic acid (PA), methacrylic acid (MAA), propylene, and unknown compounds. MeOH conversion = 8.4% (Mg/Ga-10) and 32.2% (Ga₂O₃); MMA selectivity with respect to MeOH = 15.7% (Mg/Ga-10) and 4.9% (Ga₂O₃).

redox activity required for the *in situ* dehydrogenation of MeOH.

The highest yield toward MMA (8%) was achieved on Ga₂O₃; however, a similar yield of MMA (6.6%) was obtained on the mixed metal oxide with a Mg/Ga ratio equal to 10, indicating that, indeed, Ga³⁺ promotes the desired reactions.

Both the yields of H-transfer MP products and ketones increased in the order Ga₂O₃ < Mg/Ga mixed oxides < MgO/Ga₂O₃ physical mixture < MgO, thus indicating that the activity for ketonization and H-transfer increased along with an increase in catalyst basicity. Therefore, the introduction of Ga³⁺ in Mg/Ga mixed oxides limited the occurrence of ketonization and H-transfer and enhanced catalyst selectivity toward MMA by reducing the strength and density of basic sites with respect to pure MgO (Table 1 and Figure 2a).

On the other hand, remarkably, none of the Mg-containing oxides (e.g., MgO, Mg/Ga-20 and Mg/Ga-10) showed any sign of deactivation, which, conversely, readily occurred on Ga₂O₃ (Figure 5) due to the presence of strong acidic sites.

Therefore, despite the fact that the introduction of Ga³⁺ ions into Mg/Ga mixed oxides increased their acidity compared to pure MgO (Table 1 and Figure 2b), the resulting acidic sites do not seem strong enough to cause an extensive deactivation in the short term (6–8 h) as was the case for pure Ga₂O₃. As an example, Figure 8 shows the results obtained on Mg/Ga-10 as a function of the time on stream in the same reaction conditions of Figure 7.

Another example of the stability of the Mg/Ga-10 catalyst is given in Figure S22, which depicts the results obtained as a function of the time on stream at 400 °C, W/F = 1.0 s·g/mL, and gaseous feed composition (MP/MeOH/N₂ = 1/10/89 mol %). In both cases (Figures 8 and S22), stable MMA yields over time were obtained.

As a general trend, the deactivation of the catalysts is fostered by high reaction temperatures, and such behavior is noticeable in the case of Ga₂O₃ (Figures 5 and S12); Mg/Ga-

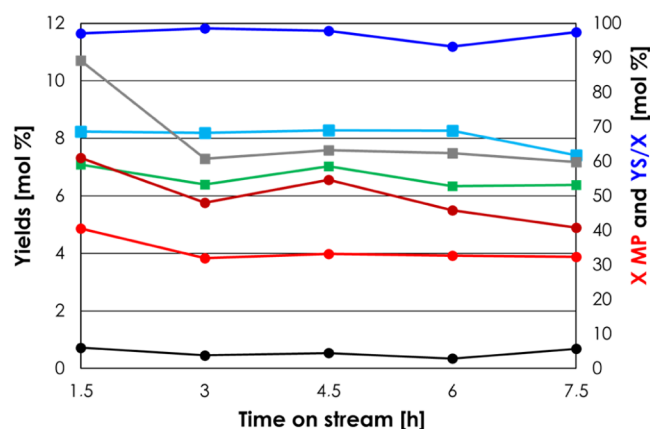


Figure 8. Catalytic activity of Mg/Ga-10. Reaction conditions: feed composition (mol %) MP/MeOH/N₂ = 1/10/89; W/F (time factor) = 1.0 s·g/mL; temperature = 425 °C. Right y-axis: MP conversion (X MP) and molar balance (YS/X). Left y-axis: product yields. Symbols: X MP (red solid circle), YS/X (solid blue circle), MMA (green solid square), the sum of the yields of H-transfer products from MP (sky blue solid square), the sum of the yields of H-transfer products from MMA (gray solid square), the sum of the yields of ketones (dark red solid circle), and others (black solid circle). “Others” includes propionic acid (PA), methacrylic acid (MAA), propylene, and unknown compounds.

10, however, showed good stability also at very high temperature, namely, 425 °C (Figure S23).

Figure 9 shows the sum of the yields of all of the possible products of hydroxymethylations (e.g., MMA, H-transfer

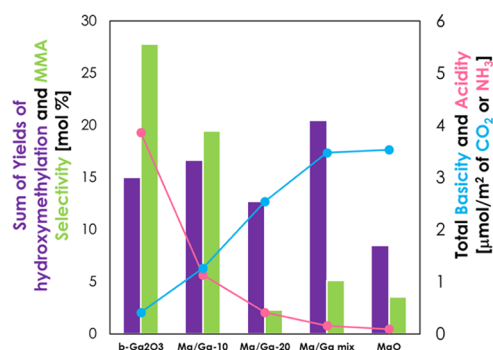


Figure 9. Catalytic activity of Ga₂O₃, Mg/Ga-10, Mg/Ga-20, Mg/Ga-mix, and MgO. Reaction conditions: feed composition (mol %) MP/MeOH/N₂ = 1/5/94; W/F (time factor) = 0.5 s·g/mL; temperature = 400 °C. Right y-axis: total basicity and total acidity. Left y-axis: product yields and selectivities. Symbols: total basicity (light blue solid circle), total acidity (pink solid circle), the sum of yields of hydroxymethylated products (purple bar), and MMA selectivity (green bar). “Hydroxymethylated products” includes MIB, IBAL, MAL, 2-MP, IB, isobutyric acid (IBA), M-3Pe, M-3Pa, DM-3Pe, and DM-3Pa.

MMA products, and methylated ketones), and the selectivity toward MMA for the same catalytic screening is depicted in Figure 7 on the left y-axis, while on the right y-axis are reported the value of total acidity and total basicity of each catalyst.

The hydroxymethylation activity depends on both the catalyst basicity (for MP activation) and the catalyst redox activity (for MeOH dehydrogenation to FAL). The comparison between the two pure oxides Ga₂O₃ and MgO, however, shows that the redox activity seems to play a major role: in fact,

the former catalyst, which shows a stronger redox activity and weaker basicity (0.41 μmol/m² of CO₂), is more active than the latter, which has a weaker redox activity and a much stronger basicity (3.53 μmol/m² of CO₂). The results obtained with Mg/Ga-20 (2.54 μmol/m² of CO₂) and Mg/Ga-10 (1.26 μmol/m² of CO₂), which possess an intermediate basicity, confirm this hypothesis: since a higher Ga³⁺ content in Mg/Ga mixed oxides reduces the density and strength of basic sites and increases the redox activity compared to MgO, the experimental activity order toward hydroxymethylations (e.g., Mg/Ga-10 > Mg/Ga-20 > MgO) can only be explained by the enhanced redox activity of the mixed metal oxides compared to MgO.

The greatest yield of hydroxymethylated products was obtained on the physical mixture MgO/Ga₂O₃ because of the simultaneous presence of a strong basicity (due to the presence of MgO) and a strong redox power (due to the presence of Ga₂O₃) in this catalyst (see Table 1). However, the selectivity toward MMA on the physical mixture was very low compared to Mg/Ga-10 (Figure 8) and Ga₂O₃ because its strong basicity triggered parasitic H-transfer reactions that consumed MMA.

CONCLUSIONS

MP gas-phase hydroxy-methylation and dehydration of MP with FAL (the latter produced *in situ* by MeOH dehydrogenation) were investigated in depth on MgO, a benchmark material for base-catalyzed reactions. The overall reaction scheme was elucidated, and it was found to consist of four main reaction pathways, namely, (1) the hydroxymethylation of MP with FAL, (2) H-transfer hydrogenations of the reactant MP, (3) H-transfer hydrogenations of the product MMA, and (4) ketonization of the reactant MP.

Bifunctional catalysts containing Ga³⁺ ions were found to be much more active and selective toward MMA than pure MgO; the investigated materials were a commercial Ga₂O₃, a physical MgO/Ga₂O₃ mixture with a Mg/Ga atomic ratio of 10, and two Mg/Ga mixed oxides with Mg/Ga atomic ratios of 10 and 20. These active and selective mixed oxides with a relatively high specific surface area (>100 m²/g) can be prepared using a simple, cheap, and easily scalable co-precipitation technique. The guest Ga³⁺ ion acted as a promoter, strongly enhancing the dehydrogenating activity toward MeOH compared to pure MgO. Moreover, the introduction of Ga³⁺ into MgO also had a strong effect in modulating catalyst surface features: both the density and the strength of basic sites were decreased, with weak acidic Lewis sites being generated at the same time.

The correlation of the acidic/basic surface properties measured by means of TPD and the evaluation of the catalytic performance of catalysts containing different amounts of Ga³⁺ made it possible to determine which features are more desirable for obtaining good MMA selectively. The best catalysts (β-Ga₂O₃ and Mg/Ga-10) were those with a strong dehydrogenating power (necessary to obtain a large excess of FAL) and weak basic sites (which are responsible for the selective hydroxymethylation of MP). On the other hand, the side reactions of H-transfer hydrogenation and MP ketonization were clearly more prominent on catalysts with strong and medium-strength basic sites (e.g., MgO and Mg/Ga-20). Strong Lewis acidic sites (which are only present on the surface of β-Ga₂O₃) were likely to be responsible for consecutive reactions such as the aldol condensation of ketones and FAL polymerization, which led to coking and deactivation of this catalyst over 18 h of time on stream;

nevertheless, β -Ga₂O₃ proved to be the most active and selective catalyst at 450 °C before deactivation. No evidence of deactivation was, instead, observed in the short term with any of the Mg-containing catalysts. To better elucidate the reaction mechanism and further confirm the structure–activity relationships identified in this study, operando X-ray absorption near-edge structure (XANES)/extended X-ray absorption fine structure (EXAFS) analyses on Ga-based catalysts have been planned for the future.

A detailed comparison between the performances of the best catalysts in this study (e.g., β -Ga₂O₃ and Mg/Ga-10) and those of the other catalytic systems reported in the literature^{3,30,31} can be found in Table S1. Ga-based material productivity is fair, situated halfway between that of the Cs/SiO₂-based catalysts^{3,30} and the Mn/MgO catalyst.³¹

The selectivity of Ga-catalysts, however, needs to be improved both by reducing the extent of the consecutive H-transfer reduction on MMA and by limiting the extent of methanol/FAL unselective decompositions, the latter representing a critical bottleneck to the applicability of the proposed strategy. Moreover, the purification of MMA from MIB, the reduction of the MeOH/MP molar ratio required to avoid ketonization, and the enhancement of process productivity represent other hurdles to overcome before a practical use could be achieved. Therefore, based on the preliminary information described in this work, future efforts will be devoted to catalyst and reaction condition optimization.

Nonetheless, if H-transfer consecutive parasitic reactions occurring on MMA were completely suppressed, yields in MMA as high as 65% at 100% MP conversion would be achieved at 425 °C over Mg/Ga-10 (Figure S23).

In conclusion, this is the first study that reports on the activity and selectivity of relatively simple and low-cost Ga-based catalytic systems for the one-pot gas-phase synthesis of MMA by means of hydroxymethylation and dehydration of MP with FAL produced *in situ* by MeOH dehydrogenation.

■ ASSOCIATED CONTENT

SI Supporting Information

The Supporting Information is available free of charge at <https://pubs.acs.org/doi/10.1021/acssuschemeng.0c07932>.

Catalyst preparation procedures, results related to blank tests, XRD of the catalytic materials, detailed product distribution for both ketonization- and H-transfer-derived compounds obtained in the reaction conditions described in the main text, a detailed description of the synthesis of the 5% Cs/SiO₂ catalyst, TGA, XPS spectra, comparison in terms of atom efficiency between the Alpha process and the one-pot process, and comparison of the obtained results with the literature (PDF)

■ AUTHOR INFORMATION

Corresponding Author

Tommaso Tabanelli – Dipartimento di Chimica Industriale “Toso Montanari”, Alma Mater Studiorum Università di Bologna, I-40136 Bologna, Italy; Consortium INSTM, Research Unit of Bologna, I-50121 Firenze, Italy; orcid.org/0000-0003-0616-8990; Email: tommaso.tabanelli@unibo.it

Authors

Jacopo De Maron – Dipartimento di Chimica Industriale “Toso Montanari”, Alma Mater Studiorum Università di Bologna, I-40136 Bologna, Italy; Consortium INSTM, Research Unit of Bologna, I-50121 Firenze, Italy

Martina Eberle – Dipartimento di Chimica Industriale “Toso Montanari”, Alma Mater Studiorum Università di Bologna, I-40136 Bologna, Italy

Fabrizio Cavani – Dipartimento di Chimica Industriale “Toso Montanari”, Alma Mater Studiorum Università di Bologna, I-40136 Bologna, Italy; Consortium INSTM, Research Unit of Bologna, I-50121 Firenze, Italy; orcid.org/0000-0002-4282-6260

Francesco Basile – Dipartimento di Chimica Industriale “Toso Montanari”, Alma Mater Studiorum Università di Bologna, I-40136 Bologna, Italy

Nikolaos Dimitratos – Dipartimento di Chimica Industriale “Toso Montanari”, Alma Mater Studiorum Università di Bologna, I-40136 Bologna, Italy

Pedro J. Maireles-Torres – Departamento de Química Inorgánica, Cristalografía y Mineralogía (Unidad Asociada al ICP-CSIC), Universidad de Málaga, E-29071 Málaga, Spain; orcid.org/0000-0002-7610-6042

Enrique Rodríguez-Castellón – Departamento de Química Inorgánica, Cristalografía y Mineralogía (Unidad Asociada al ICP-CSIC), Universidad de Málaga, E-29071 Málaga, Spain; orcid.org/0000-0003-4751-1767

Complete contact information is available at: <https://pubs.acs.org/doi/10.1021/acssuschemeng.0c07932>

Notes

The authors declare no competing financial interest.

■ ACKNOWLEDGMENTS

E.R.-C. thanks project RTI2018-099668-BC22 of Ministerio de Ciencia, Innovación y Universidades and FEDER funds. The INSTM (Consorzio Interuniversitario per la Scienza e Tecnologia dei Materiali), Florence, is acknowledged for the Ph.D. grant to J.D.M.

■ REFERENCES

- (1) Stickler, M.; Rhein, T. Polymethacrylates. *Ullmann's Encycl. Ind. Chem.* **2000**, *29*, 341–354.
- (2) Darabi Mahboub, M. J.; Dubois, J.; Cavani, F.; Rostamizadeh, M.; Patience, G. S. Catalysis for the synthesis of methacrylic acid and methyl methacrylate. *Chem. Soc. Rev.* **2018**, *47*, 7703–7738.
- (3) Jackson, S. D.; Johnson, D. W.; Scott, J. D.; Kelly, G. J.; Williams, B. P. Catalysts for the Production of Unsaturated Acids or Esters. US6,544,924B1, 2003.
- (4) Tindale, N.; Eastham, G. R. A Continuous Process for the Carbonylation of Ethylene. WO2013093472A1, 2011.
- (5) IARC. *Formaldehyde, 2-Butoxyethanol and 1-tert-butoxypropan-2-ol*, IARC Monographs on the Evaluation of Carcinogenic Risks to Humans, No. 88; International Agency for Research on Cancer, 2006; pp 39–280.
- (6) Molino, A.; Larocca, V.; Chianese, S.; Musmarra, D. Biofuels production by biomass gasification: a review. *Energies* **2018**, *11*, No. 811.
- (7) Morschbacker, A. Bio-ethanol based ethylene. *Polym. Rev.* **2009**, *49*, 79–84.
- (8) Dubois, J. Method for Manufacturing a Biomass-Derived Methyl Methacrylate. US20,110,287,991A1, 2011.

- (9) Johnson, D. W.; Eastham, G. R.; Poliakov, M.; Huddle, T. H. Process for the Production of Methacrylic Acid and Its Derivatives and Polymers Produced Therefrom. US9,174,913B2, 2015.
- (10) Ciriminna, R.; Della Pina, C.; Rossi, M.; Pagliaro, M. Understanding the glycerol market. *Eur. J. Lipid Sci. Technol.* **2014**, *116*, 1432–1439.
- (11) Nakagawa, Y.; Tamura, M.; Tomishige, K. Perspective on catalyst development for glycerol reduction to C3 chemicals with molecular hydrogen. *Res. Chem. Intermed.* **2018**, *44*, 3879–3903.
- (12) Bandinelli, C.; Lambiase, B.; Tabanelli, T.; De Maron, J.; Dimitratos, N.; Basile, F.; Concepcion, P.; Nieto, J. M. L.; Cavani, F. A study of the oxidehydration of 1,2-propanediol to propanoic acid with bifunctional catalysts. *Appl. Catal., A* **2019**, *582*, No. 117102.
- (13) Zhu, Y.; Li, J.; Tan, M.; Liu, L.; Jiang, L.; Sun, J.; Lee, P.; Du, G.; Chen, J. Optimization and scale-up of propionic acid production by propionic acid-tolerant *Propionibacterium Acidipropionici* with glycerol as the carbon source. *Bioresour. Technol.* **2010**, *101*, 8902–8906.
- (14) Fasolini, A.; Cespi, D.; Tabanelli, T.; Cucciniello, R.; Cavani, F. Hydrogen from renewables: a case study of glycerol reforming. *Catalysts* **2019**, *9*, No. 722.
- (15) Fasolini, A.; Cucciniello, R.; Paone, E.; Mauriello, F.; Tabanelli, T. A short overview on the hydrogen production via aqueous phase reforming (APR) of Cellulose, C6-C5 Sugars and Polyols. *Catalysts* **2019**, *9*, No. 917.
- (16) Li, B.; Yan, R.; Wang, L.; Diao, Y.; Li, Z.; Zhang, S. Synthesis of methyl methacrylate by aldol condensation of methyl propionate with formaldehyde over acid-base bifunctional catalysts. *Catal. Lett.* **2013**, *143*, 829–838.
- (17) Ai, M. Vapor-phase aldol condensation of formaldehyde with propionic acid on vanadium pentoxide-phosphorus pentoxide. *Appl. Catal.* **1988**, *36*, 221–230.
- (18) Spivey, J. J.; Gogate, M. R.; Zoeller, J. R.; Colberg, R. D. Novel catalysts for the environmentally friendly synthesis of methyl methacrylate. *Ind. Eng. Chem. Res.* **1997**, *36*, 4600–4608.
- (19) Reuss, G.; Disteldorf, W.; Gamer, A. O.; Hilt, A. Formaldehyde. *Ullmann's Encycl. Ind. Chem.* **2000**, *15*, 735–768.
- (20) Folliard, V.; Postole, G.; Marra, L.; Dubois, J.; Auroux, A. Sustainable acrolein production from bio-alcohols on spinel catalysts: influence of magnesium substitution by various transition metals (Fe, Zn, Co, Cu, Mn). *Appl. Catal., A* **2020**, *608*, No. 117871.
- (21) Dubois, J.; Capron, M.; Dumeignil, F. Method for Directly Synthesizing Unsaturated Aldehydes from Alcohol Mixtures. US9,365,478B2, 2016.
- (22) Gaertner, C. A.; Serrano-Ruiz, J. C.; Braden, D. J.; Dumesic, J. A. Catalytic coupling of carboxylic acids by ketonization as a processing step in biomass conversion. *J. Catal.* **2009**, *266*, 71–78.
- (23) Fouquet, G.; Merger, F.; Platz, R.; Baer, K. Manufacture of Methacrylic Acid and Methyl Methacrylate. US4,118,588, 1978.
- (24) Himeno, Y.; Ken, O.; Masahide, K. Dehydration of Water Containing Source of Formaldehyde, and a Method for Producing an Ethylenically Unsaturated Carboxylic Ester. US20,150,053,616A1, 2015.
- (25) Usachev, N. Y.; Krukovsky, I. M.; Kanaev, S. A. The nonoxidative methanol dehydrogenation to formaldehyde (a review). *Pet. Chem.* **2004**, *44*, 379–394.
- (26) Lausche, A. C.; Hummelshøj, J. S.; Abild-Pedersen, F.; Studt, F.; Nørskov, J. K. Application of a new informatics tool in heterogeneous catalysis: analysis of methanol dehydrogenation on transition metal catalysts for the production of anhydrous formaldehyde. *J. Catal.* **2012**, *291*, 133–137.
- (27) Tabanelli, T.; Passeri, S.; Guidetti, S.; Cavani, F.; Lucarelli, C.; Cargnoni, F.; Mella, M. A cascade mechanism for a simple reaction: the gas-phase methylation of phenol with methanol. *J. Catal.* **2019**, *370*, 447–460.
- (28) Cavani, F.; Maselli, L.; Passeri, S.; Lercher, J. A. Catalytic methylation of phenol on MgO - surface chemistry and mechanism. *J. Catal.* **2010**, *269*, 340–350.
- (29) Ballarini, N.; Cavani, F.; Maselli, L.; Montaletti, A.; Passeri, S.; Scagliarini, D.; et al. The transformations involving methanol in the acid- and base-catalyzed gas-phase methylation of phenol. *J. Catal.* **2007**, *251*, 423–436.
- (30) Ai, M. Formation of methyl methacrylate from methyl propionate and methanol. *Catal. Today* **2006**, *111*, 398–402.
- (31) Ueda, W. Catalytic synthesis of α,β -unsaturated compounds over solid-bases using methanol for C=C bond formation. *Sekiyu Gakkaishi* **1993**, *36*, 421–435.
- (32) Bailey, O. H.; Montag, R. A.; Yoo, J. S. Methacrylic acid synthesis: I. Condensation of propionic acid with formaldehyde over alkali metal cation on silica catalysts. *Appl. Catal., A* **1992**, *88*, 163–177.
- (33) Wang, F.; Ta, N.; Shen, W. MgO nanosheets, nanodisks, and nanofibers for the Meerwein–Ponndorf–Verley reaction. *Appl. Catal., A* **2014**, *475*, 76–78.
- (34) Cavani, F.; Maselli, L.; Scagliarini, D.; Flego, C.; Perego, C. How basic properties of MgO-based mixed oxides affect the catalytic performance in gas-phase and liquid-phase methylation of m-cresol. *Stud. Surf. Sci. Catal.* **2005**, *155*, 167–177.
- (35) Tabanelli, T.; Monti, E.; Cavani, F.; Selva, M. The design of efficient carbonate interchange reactions with catechol carbonate. *Green Chem.* **2017**, *19*, 1519–1528.
- (36) Tabanelli, T.; Giliberti, C.; Mazzoni, R.; Cucciniello, R.; Cavani, F. An innovative synthesis pathway to benzodioxanes: the peculiar reactivity of glycerol carbonate and catechol. *Green Chem.* **2019**, *21*, 329–338.
- (37) Glebov, L. S.; Shuikin, A. N.; Kliger, G. A. Heterogeneous catalytic transformation of isobutyl benzoate by the inverse Tishchenko reaction. *Russ. Chem. Bull.* **1994**, *43*, 1417–1419.
- (38) Ruiz, J. R.; Sanchidrian, C. J.; Hidalgo, J. M.; Marinas, J. M. Reduction of ketones and aldehydes to alcohols with magnesium–aluminum mixed oxide and 2-propanol. *J. Mol. Catal. A: Chem.* **2006**, *246*, 190–194.
- (39) Aramendia, M. A.; Borau, V.; Jimenez, C.; Marinas, A.; Marinas, J. M.; Porras, A.; Urbano, F. J. Gas-phase hydrogen-transfer reduction of acrolein using 2-propanol over MgO/B₂O₃ and SiO₂/AlPO₄ catalysts. *Catal. Lett.* **1998**, *50*, 173–177.
- (40) Taylor, J. D.; Jenni, M. M.; Peters, M. W. Dehydration of fermented isobutanol for the production of renewable chemicals and fuels. *Top. Catal.* **2010**, *53*, 1224–1230.
- (41) Grazia, L.; Lolli, A.; Folco, F.; Zhang, Y.; Albonetti, S.; Cavani, F. Gas-phase cascade upgrading of furfural to 2-methylfuran using methanol as a H-transfer reactant and MgO based catalysts. *Catal. Sci. Technol.* **2016**, *6*, 4418–4427.
- (42) Pasini, T.; Lolli, A.; Albonetti, S.; Cavani, F.; Mella, M. Methanol as a clean and efficient H-transfer reactant for carbonyl reduction: scope, limitations, and reaction mechanism. *J. Catal.* **2014**, *317*, 206–219.
- (43) Gyngazova, M. S.; Grazia, L.; Lolli, A.; Innocenti, G.; Tabanelli, T.; Mella, M.; Albonetti, S.; Cavani, F. Mechanistic insights into the catalytic transfer hydrogenation of furfural with methanol and alkaline earth oxides. *J. Catal.* **2019**, *372*, 61–73.
- (44) Kumar, R.; Enjamuri, N.; Shah, S.; Al-Fatesh, A. S.; Bravo-Suarez, J. J.; Chowdhuri, B. Ketonization of oxygenated hydrocarbons on metal oxide based catalysts. *Catal. Today* **2018**, *302*, 16–49.
- (45) Tabanelli, T.; Cocchi, S.; Gumina, B.; Izzo, L.; Mella, M.; Passeri, S.; Cavani, F.; Lucarelli, C.; Schütz, J.; Bonrath, W.; Netscher, T. Mg/Ga mixed-oxide catalysts for phenol methylation: outstanding performance in 2,4,6-trimethylphenol synthesis with co-feeding of water. *Appl. Catal., A* **2018**, *552*, 86–97.
- (46) Zheng, B.; Hua, W.; Yue, Y.; Gao, Z. Dehydrogenation of propane to propene over different polymorphs of gallium oxide. *J. Catal.* **2005**, *232*, 143–151.
- (47) Nakagawa, K.; Okamura, M.; Ikenaga, N.; Suzuki, T.; Nakagawa, K.; et al. Dehydrogenation of ethane over gallium oxide in the presence of carbon dioxide. *Chem. Commun.* **1998**, *3*, 1025–1026.

(48) Gliński, M.; Zalewski, G.; Burno, E.; Jerzak, A. Catalytic ketonization over metal oxide catalysts XIII: comparative measurements of activity of oxides of 32 chemical elements in ketonization of propanoic acid. *Appl. Catal., A* **2014**, *470*, 278–284.

(49) Gelius, U.; Heden, P. F.; Hedman, J.; Lindberg, B. J.; Manne, R.; Nordberg, R.; Nordling, C.; Siegbahn, K. Molecular spectroscopy by means of ESCA III: carbon compounds. *Phys. Scr.* **1970**, *2*, 70–80.

(50) Wheeler, V. D.; Shahin, D. I.; Tadjer, M. J.; Eddy, C. R., Jr. Band alignments of atomic layer deposited ZrO₂ and HfO₂ high-k dielectrics with (−201) β-Ga₂O₃. *ECS J. Solid State Sci. Technol.* **2017**, *6*, Q3052.

(51) López, G. P.; Castner, D. G.; Ratner, B. D. XPS O 1s binding energies for polymers containing hydroxyl, ether, ketone and ester groups. *Surf. Interface Anal.* **1991**, *17*, 267–272.

(52) Zatsepin, D. A.; Boukhvalov, D. W.; Zatsepin, A. F.; Kuznetsova, Y. A.; Godova, D.; Shur, V. Y.; Esin, A. A. Atomic structure, electronic states, and optical properties of epitaxially grown β-Ga₂O₃ layers. *Superlattices Microstruct.* **2018**, *120*, 90–100.

(53) Rudnick, R. L.; Gao, S. Composition of the continental crust. *Treatise Geochem.* **2014**, *4*, 1–51.

(54) Frenzel, M.; Ketris, M. P.; Seifert, T.; Gutzmer, J. On the current and future availability of gallium. *Resour. Policy* **2016**, *47*, 38–50.

(55) Ballarini, N.; Cavani, F.; Maselli, L.; Passeri, S.; Rovinetti, S. Mechanistic studies of the role of formaldehyde in the gas-phase methylation of phenol. *J. Catal.* **2008**, *256*, 215–225.